Gulf General Atomic
Incorporated
P.O. Box 608, San Diego, California 92112

AEC RESEARCH AND
DEVELOPMENT REPORT

GA-8380

SESH - A FORTRAN IV CODE FOR CALCULATING THE SELF-SHIELDING AND MULTIPLE SCATTERING EFFECTS FOR NEUTRON CROSS SECTION DATA INTERPRETATION IN THE UNRESOLVED RESONANCE REGION

by

F. H. Fröhner

Prepared under
Contract AT(04-3)-167
Project Agreement N. 11
for the
San Francisco Operations Office
U. S. Atomic Energy Commission

Gulf General Atomic Project 221

January 3, 1968

CONTENTS

1. INTRODUCTION

The FORTRAN IV code SESH, which is described in this report, uses Monte Carlo methods to calculate resonance self-shielding and multiple scattering effects as needed for the interpretation of neutron capture and self-indication data in the energy region of unresolved resonances. The code also computes average transmissions for the analysis of neutron transmission data in the unresolved-resonance region. These calculations are based on level statistics. Resonance spins, average spacings, strength functions, and average radiation widths, together with sample specifications, constitute the principal input. Inelastic scattering can be treated approximately. Slab-sample and spherical-shell sample geometries can be handled. In the slab sample case the sample is taken to be a cylindrical disc, with the cylinder axis parallel to the neutron beam direction, and with the intensity uniformly distributed over the disc area. For more technical details see Section 6.

The terms "unresolved-resonance region," "resonance self-protection," "average transmission," etc., as used here need some explanation: generally the so-called cross-section experiments - total or partial - do not yield the cross sections directly, but more or less complicated functionals of the cross sections. Moreover, at sufficiently high energies one measures only averages of these functionals over many resonances, because of resonance overlap due to Doppler broadening and limited energy resolution. The energy region, where individual resonances are no longer resolved instrumentally, but where the Doppler-broadened cross sections still have definite resonance structure, will be called the "unresolved-resonance region" (see Fig. 1). With modern time-of-flight

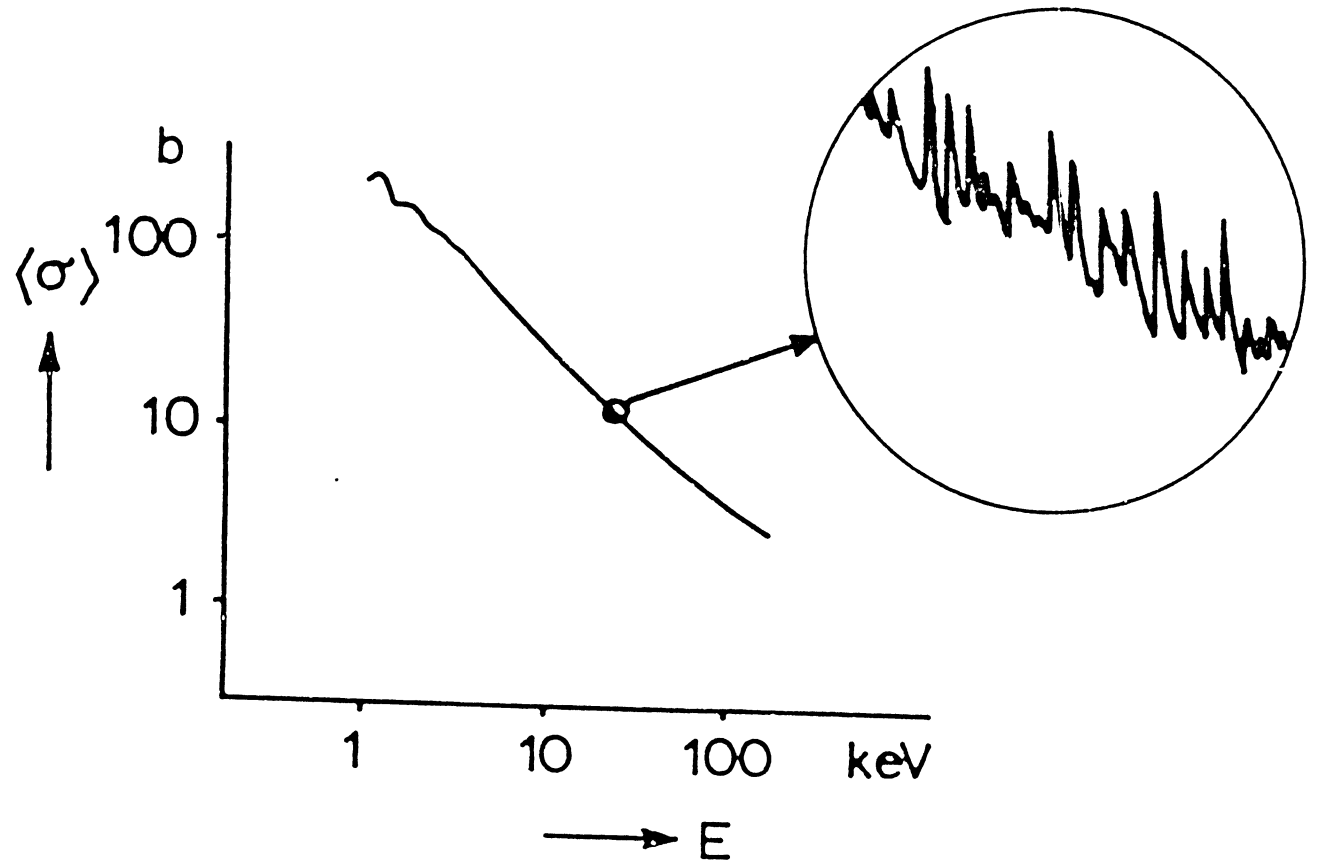

Fig. 1. Schematic illustration of experimental cross section in the unresolved-resonance region. In the circle a blow-up is shown of what would be seen with ideal resolution and statistics.

equipment this region lies typically above a few keV for heavy nuclei, and above a few hundred keV for light nuclei.

Interpretation of capture data in the unresolved-resonance region invariably necessitates the calculation of resonance self-shielding and multiple scattering. Resonance self-shielding (or self-protection) is caused by the resonance structure of the cross sections in conjunction with the non-linear relationship between total cross section and transmission. Multiple scattering refers to events in which a neutron is captured only after one or more scattering interactions in the sample. Both effects increase in magnitude with sample thickness. Transmission data are unaffected by multiple scattering, but not by the resonance structure of the total cross section.

Time-of-flight experiments are usually performed in disc geometry: A well-collimated neutron beam hits a slab sample of uniform thickness. On the other hand, sphere transmission (or better, sphere absorption) experiments are performed with a sample in the form of a spherical shell which surrounds an isotropic neutron source (or detector, see Ref. 1).

Dresner[2] was the first to attack the problem of self-shielding and multiple scattering for neutron capture data taken in slab geometry. He derived approximations for the case of an isolated symmetric resonance. Macklin[3] gave relatively simple analytical expressions approximating Dresner's results, and also expressions for spherical-shell geometry. Dresner's and Macklin's results depend on a number of assumptions that are generally justified at low energies and for thin samples. However, at higher energies and for thick samples their formulae become questionable. Furthermore, one must average their single-level expressions over the width and spacing distributions. Bogart and Semler[4, 5] in their analysis of sphere transmission data avoided these difficulties by using Monte Carlo techniques to generate realistic cross-section distributions. Essentially the same approach is used in the present work.

Before describing the code in detail we shall review the relevant cross-section formulae and resonance statistics.

SLBW totale $\sigma_c = 4\pi \lambda_c^2 g_c \left\{ \sin^2 \varphi_c + \frac{\Gamma_c}{\Gamma} (\psi \cos 2\varphi_c + \chi \sin 2\varphi_c) \right\}$

sachant $\sigma_p = 4\pi \lambda_c^2 g_c \sin^2 \varphi_c$ et $\sigma_0 = 4\pi \lambda_c^2 g_c$

$\Leftrightarrow \sigma_c = \sigma_0 \left(\frac{\Gamma_c}{\Gamma} (\psi \cos 2\varphi_c + \chi \sin 2\varphi_c) \right) + \sigma_p$

hyp : capture et fission négligeable Γ & Γ_c

$\Rightarrow \sigma_c = \sigma_0 (\psi \cos 2\varphi_c + \chi \sin 2\varphi_c) + \sigma_p$

2. NEUTRON CROSS SECTION RESONANCES

We shall describe resonance cross sections formally by simply adding single-level Breit-Wigner terms to the potential scattering cross section, neglecting potential (direct) capture. In this way, level-level interference effects other than those caused by mere overlap of single-level Breit-Wigner resonances will be neglected. Feshbach, Porter and Weisskopf[6] showed that this approximation is good at relatively low energies ($\chi << R$) and for reasonably well isolated resonances ($\langle \Gamma \rangle << D$). In evaluating Doppler broadening we treat slowly varying functions of the neutron energy E as local constants. Thus, one arrives at the following formulae for the Doppler-broadened cross sections of a monotope:

total cross section,

$$\sigma = \sum_\lambda [\sigma_0 (\psi \cos 2\xi - \varphi \sin 2\xi)]_\lambda + \sigma_p ; \qquad (1)$$

capture cross section,

$$\sigma_\gamma = \sum_\lambda \left[\sigma_0 \frac{\Gamma_\gamma}{\Gamma} \psi \right]_\lambda ;$$

SLBW $\sigma_\gamma = \sigma_0 \frac{\Gamma_c \Gamma_\gamma}{\Gamma^2} \psi \simeq \sigma_0 \frac{\Gamma_\gamma}{\Gamma}$ hyp $\Gamma \sim \Gamma_c$ (2)

cross section for inelastic scattering,

$$\sigma_{n'} = \sum_\lambda \left[\sigma_0 \frac{\Gamma_{n'}}{\Gamma} \psi \right]_\lambda ;$$

$\sigma_{n'} = \sigma_0 \frac{\Gamma_c \Gamma_{n'}}{\Gamma^2} \psi \simeq \sigma_0 \frac{\Gamma_{n'}}{\Gamma} \psi$ (3)

potential scattering cross section,

$$\sigma_p = 4\pi\lambda\!\!\!^{-2} \sum_{l=0}^{\infty} (2l+1) \sin^2 \xi_l \ ; \tag{4}$$

and

$$\sigma_0 = 4\pi\lambda\!\!\!^{-2} g_J \frac{\Gamma_n}{\Gamma} \ . \tag{5}$$

The center-of-mass neutron wave length was denoted by $2\pi\lambda\!\!\!^{-}$, the partial widths for radiative capture, elastic, and inelastic scattering by Γ_γ, Γ_n, $\Gamma_{n'}$, resp., the total width by $\Gamma = \Gamma_\gamma + \Gamma_n + \Gamma_{n'}$. The spin factor $g_J = (1/2)(2J+1)/(2I+1)$ is the statistical weight of compound states with spin $J\hbar$ if $I\hbar$ is the ground state spin of the target nucleus. Processes other than capture, elastic, or inelastic scattering will be considered as negligible, so that the cross section for elastic scattering is given by

$$\sigma_n = \sigma - \sigma_\gamma - \sigma_{n'} \ . \tag{6}$$

The potential-scattering phase shifts ξ will be taken as the hard-sphere values for an effective interaction radius R, depending only on the orbital momentum quantum number l, $\xi = \xi_l$:

s-wave

$$\xi_0 = -R/\lambda\!\!\!^{-} \ ; \tag{7.0}$$

p-wave

$$\xi_1 = \xi_0 - \operatorname{arc\,tg} \xi_0 \ ; \tag{7.1}$$

d-wave

$$\xi_2 = \xi_0 - \operatorname{arc\,tg} \frac{3\xi_0}{3-\xi_0^2} \ ; \tag{7.2}$$

f-wave

$$\xi_3 = \xi_0 - \operatorname{arc\,tg} \frac{15\xi_0 - \xi_0^3}{15 - 6\xi_0^2} \quad ; \tag{7.3}$$

etc.

The sums in Eqs. 1 - 3 are to be extended over all resonances that contribute appreciably to the cross section at the energy of the incoming neutron.

The functions ψ and φ are the familiar Doppler shape functions:[7]

$$\psi(x,\beta) = \frac{1}{\beta\sqrt{\pi}} \int_{-\infty}^{\infty} \exp\left[-\left(\frac{x-y}{\beta}\right)^2\right] \frac{dy}{1+y^2} \quad , \tag{8}$$

$$\varphi(x,\beta) = \frac{1}{\beta\sqrt{\pi}} \int_{-\infty}^{\infty} \exp\left[-\left(\frac{x-y}{\beta}\right)^2\right] \frac{y\,dy}{1+y^2} \quad , \tag{9}$$

with

$$x \equiv \frac{E-E_0}{\Gamma/2} \tag{10}$$

and

$$\beta \equiv \frac{\Delta}{\Gamma/2} \equiv \frac{4}{\Gamma}\left(\frac{EkT}{A}\right)^{1/2} \quad . \tag{11}$$

Here E_0 denotes the resonance energy, Δ the Doppler width, kT the effective temperature of the sample material (see Ref. 8) in energy units, and A the mass number or, more precisely, the mass of the target nucleus in units of the neutron mass. We shall need the following property of the Doppler shape functions:

$$\int_{-\infty}^{\infty} \psi(x,\beta)\,dx = \pi \quad , \quad \int_{-\infty}^{\infty} \varphi(x,\beta)\,dx = 0 \quad . \tag{12),(13}$$

We shall also need the concept of reduced width. The neutron width of a given resonance can be written as

$$\Gamma_n = \sqrt{\frac{E}{E_1}} \sum_{\ell, s} v_\ell (E) \Gamma^{\ell}_{n, s} , \tag{14}$$

where E_1 is the conventional reference energy of 1 eV, s is the channel spin, and $\Gamma^{\ell}_{n, s}$ is the reduced neutron width for the (ℓ, s)-channel. The v are hard-sphere penetration factors describing the effect of the centrifugal barrier:

s-wave

$$v_0 = 1 ; \tag{15.0}$$

p-wave

$$v_1 = \frac{\xi_0^2}{1+\xi_0^2} ; \tag{15.1}$$

d-wave

$$v_2 = \frac{\xi_0^4}{9+3\xi_0^2+\xi_0^4} ; \tag{15.2}$$

f-wave

$$v_3 = \frac{\xi_0^6}{225+45\xi_0^2+6\xi_0^4+\xi_0^6} ; \tag{15.3}$$

etc.

3. LEVEL STATISTICS

3.1 Width Distributions

The first important distribution in level statistics is the Porter-Thomas distribution of the reduced channel widths Γ_c:[9]

$$p(\Gamma_c)d\Gamma_c = \frac{e^{-x}}{\sqrt{\pi x}}\,dx \quad \text{with} \quad x = \frac{1}{2}\,\frac{\Gamma_c}{\langle\Gamma_c\rangle}\,, \tag{21}$$

where $\langle\Gamma_c\rangle$ is the average width. (!) this is thrue only for χ^2 $\nu = 1$!!!

One example of Γ_c is the reduced neutron width $\Gamma^{\ell}_{n,sJ}$, which is proportional to the probability for reemission of a neutron from the compound state with spin J and parity $\Pi = (-)^{\ell}$ into a channel characterized by the angular momentum quantum numbers ℓ and s of the outgoing neutron. Another example is the reduced radiation width, i.e., the width for photon emission into a given channel characterized by transition energy, multipole character, and polarization state of the photon. A third example is the reduced width for inelastic scattering of a neutron, the exit channel being now characterized by the excitation or the residual nucleus and by the angular momentum quantum numbers ℓ and s of the outgoing neutron. The total reduced width of a given resonance for each of these three processes is a sum over partial reduced widths, with one sum term for each open channel (compare Eq. 14). The number of open channels of comparable importance is large in the case of photon emission because usually there are many transitions possible to lower-lying states of the compound nucleus. According to the central limit theorem of statistics, the distribution of the total reduced radiation widths for a given level sequence (J^{Π}) is then quite narrow. Therefore, it may be approximated by a δ-distribution; in other words the same total reduced

radiation width can be assumed for all resonances of a given level sequence. This is consistent with experimental evidence. Furthermore, the radiation width will be regarded as a function of parity only. (See e.g., Ref. 10):

$$\Gamma_{\gamma,\ell J} = \Gamma_{\gamma,\ell} = \langle \Gamma_{\gamma,\ell} \rangle = \langle \Gamma_{\gamma,\ell+2} \rangle \quad \text{etc.} \tag{22}$$

The energy dependence of Γ_γ is slow, so that we can neglect it locally, i.e., in the energy interval in which the average is calculated. The energy dependence over larger energy ranges is discussed in Section 6.3 (Eqs. 108, 109, 110).

The assumption of many open channels with comparable importance and therefore of local constancy will also be used with respect to the width for inelastic scattering:

$$\Gamma_{n',\ell J} = \langle \Gamma_{n',\ell J} \rangle \quad \text{locally.} \tag{23}$$

This approximation is expected to be good at relatively high energies, where many states of the residual nucleus can be excited. At low energies it is not justified since only a few, if any, exit channels are open. However, at those energies inelastic scattering is relatively unimportant ($\Gamma_{n'} << \Gamma$) and the use of an approximate distribution for Γ_n, has little effect.

The number of open channels for elastic neutron scattering is usually quite small. At low energies only the lowest value of ℓ need be considered because of the effect of the centrifugal barrier. This means that the reduced neutron width at low energies is practically equal to

$$\Gamma^{\ell}_{n,J} = \begin{cases} \Gamma^{\ell}_{n,\frac{1}{2}J} & \text{for} \quad N_{\ell J} = 1 \quad (I = 0) \\ \Gamma^{\ell}_{n,s_+ J} + \Gamma^{\ell}_{n,s_- J} & \text{"} \quad N_{\ell J} = 2 \quad (I > 0) \end{cases} \tag{24}$$

where $s_\pm = I \pm \frac{1}{2}$, and where ℓ is the lowest possible value of the orbital angular momentum quantum number. Consequently, the distribution of reduced neutron widths for $I = 0$ is simply the Porter-Thomas distribution

(χ^2-distribution with one degree of freedom), Eq. 21. The distribution for $I > 0$ is the exponential distribution (χ^2-distribution with two degrees of freedom).

$$p(\Gamma^{\ell}_{n,J})d\Gamma^{\ell}_{n,J} = e^{-x}dx, \quad \text{with } x = \frac{1}{2}\frac{\Gamma^{\ell}_{n,J}}{\langle \Gamma^{\ell}_{n,J} \rangle} , \tag{25}$$

if the averages of the two underlying Porter-Thomas distributions are assumed equal:

$$\langle \Gamma^{\ell}_{n,s_+J} \rangle = \langle \Gamma^{\ell}_{n,s_-J} \rangle \equiv \frac{1}{2} \langle \Gamma^{\ell}_{n,J} \rangle . \tag{26}$$

This assumption is consistent with experimental evidence[11] and will be used from here on. At higher energies it becomes necessary to include contributions from the next higher partial wave of the same parity. For example the so-called s-wave resonances sometimes can be excited also by d-wave neutrons, and one must use*

$$\Gamma_n = (E/E_1)^{1/2}(\Gamma^0_n v_0 + \Gamma^2_n v_2) . \tag{27}$$

For our purposes it will be sufficient to include the partial waves with $\ell \leq 3$ only.

3.2 Spacing Distribution

The second basic distribution in level statistics is the Wigner distribution,

$$p(D)dD = 2xe^{-x^2}dx \quad \text{with} \quad x = \frac{\sqrt{\pi}}{2}\frac{D}{D_{\ell J}} , \tag{28}$$

*Note: The superscript of the reduced width denotes ℓ, it is not an exponent.

which governs the nearest-neighbor spacing D within a given level sequence (J^{Π}, $\Pi = (-)^{\ell}$). $D_{\ell J}$ is the average spacing.

From thermodynamical statistics one can derive the following J-dependence of $D_{\ell J}$ at high excitation energies:[13]

$$D_{\ell J} = C_1(2J+1)^{-1} \exp\left[-C_2(2J+1)^2\right] . \tag{29}$$

Empirical evidence shows that C_2 is usually so small that one can use the approximation

$$D_{\ell J} = C_1(2J+1)^{-1} \tag{30}$$

where C_1 does not depend on ℓ, i.e., on the parity. The observable spacing for all levels with a given ℓ regardless of J is

$$D_\ell = \left[\sum_J D_{\ell J}^{-1}\right]^{-1} . \tag{31}$$

Using the definition of the spin factor, $g_J = (1/2)(2J+1)/(2I+1)$, and Eq. 30, one can show that for any ℓ and J

$$g_J D_{\ell J} = D_\ell \sum_{J'} g_{J'} = D_0 . \tag{32}$$

The sum runs over all values of the compound spin which are compatible with ℓ. From here on we shall use D_J instead of $D_{\ell J}$ because of the assumed parity-independence of C_1, Eq. 30.

The energy dependence of D_J will be taken as

$$D_J(E) = D_J(0)\, e^{-E/\Theta} , \tag{33}$$

where Θ is the nuclear temperature in energy units.[14]

3.3 Strength Functions

The strength function for the (J, ℓ, s)-channel is defined as the ratio $\langle \Gamma^{\ell}_{n,sJ} \rangle / D_J$. It will be assumed to be independent of I and s, which seems to be consistent with existing empirical evidence,[14] except possibly for nuclei with I = 3/2 (see Refs. 15, 16). Thus we write

$$S_\ell = S_{\ell Js} = \frac{\langle \Gamma^{\ell}_{n,sJ} \rangle}{D_J} \quad . \tag{34}$$

The average reduced neutron width for the ℓ-wave is then, according to Eq. 26.

$$\langle \Gamma^{\ell}_{n,J} \rangle = N_{\ell J} D_J S_\ell \quad . \tag{35}$$

The strength function defined in this way can be found from individual reduced widths measured for a sufficient number of resolved resonances as

$$S_\ell = \frac{1}{(2\ell+1)\Delta E} \sum_\lambda (g\Gamma_n)_\lambda \quad . \tag{36}$$

The sum runs over all ℓ-wave resonances in the interval ΔE, which, of course, must be chosen large enough so that it contains a statistically meaningful sample of ℓ-wave resonances (see e.g., Ref. 17, where tables of S_0 are given). Equation 36 follows directly from Eq. 34 and from the identity

$$\sum_J N_{\ell J} g_J = 2\ell+1 \quad , \tag{37}$$

where the sum runs over all values of J which are compatible with ℓ.

The optical model can be used to calculate estimates of S_ℓ. The maxima of S_ℓ (as a function of E or A) found in such calculations correspond to single-particle resonances. They are very broad ($\sim$ 2 MeV) and have such spacings ($\sim$ 10 MeV) that for our purposes S_ℓ can be considered as a constant.

4. STATISTICAL AVERAGES

4.1 Cross Section Averages

We define the average total cross section as

$$\langle \sigma \rangle = \frac{1}{\Delta E} \int_{\Delta E} dE\, \sigma(E) \quad , \tag{38}$$

where the interval ΔE is to be chosen so wide that it contains a statistically meaningful sample of resonances of each J^{Π}-sequence.

Inserting Eq. 1 in Eq. 38 and using Eq. 36 one finds

$$\langle \sigma \rangle = 2\pi^2 \lambda\!\!\!^{-}_1 \sum_{l=0}^{\infty} (2l+1) S_l v_l \cos 2\xi_l + \sigma_p \quad , \tag{39}$$

where $2\pi\lambda\!\!\!^{-}_1$ is the center-of-mass wave length corresponding to $E_1 = 1$ eV. In deriving Eq. 39 we used

$$\int_{\Delta E} dE \ldots \approx \frac{\Gamma}{2} \int_{-\infty}^{\infty} dx \ldots$$

(for the definition of x see Eq. 10), which is equivalent to the assumption that the resonances are narrow compared with the energy interval ΔE. (ΔE can be thought of as the width characterizing the energy resolution of a data point). We also used the integrals (12) and (13) over the Doppler shape functions. Furthermore, the sum over all resonances of a given sequence was replaced by the average resonance contribution (Porter-Thomas average) times the number of such resonances in ΔE. This number is, of course,

$\Delta E/D_J$. Slowly varying functions of E were treated as constants.

In exact analogy one finds for the average capture cross section

$$\langle \sigma_\gamma \rangle = 2\pi^2 \lambda^2 \sum_{J,\ell} g_J \frac{\Gamma_{\gamma,\ell}}{D_J} \left\langle \frac{\Gamma_n}{\Gamma} \right\rangle_{\ell J} , \tag{40}$$

where $\langle \ldots \rangle_{\ell J}$ denotes an average over the distributions of the partial widths for elastic and for inelastic scattering. Assuming that $\Gamma_{n'}$ is essentially constant from level to level (see Sect. 3.1.) and using only the lowest ℓ-value in the calculation of Γ_n one can evaluate the width average explicitly.

For $N_{\ell J} = 1$ one finds

$$\left\langle \frac{\Gamma_n}{\Gamma} \right\rangle_{\ell J} = 1 - \psi(0, \beta_{\ell J})$$

$$= 1 - \sqrt{\pi}\, \beta_{\ell J}^{-1} \exp(\beta_{\ell J}^{-2}) \operatorname{erfc}(\beta_{\ell J}^{-1}) , \tag{41}$$

where

$$\beta_{\ell J} = \left(\frac{2 \langle \Gamma_n \rangle_{\ell J}}{\Gamma_{\gamma,\ell} + \langle \Gamma_{n'} \rangle_{\ell J}} \right)^{1/2} . \tag{42}$$

For $N_{\ell J} = 2$ one gets

$$\left\langle \frac{\Gamma_n}{\Gamma} \right\rangle_{\ell J} = 1 - \gamma_{\ell J} \exp(\gamma_{\ell J})\, \mathrm{Ei}(-\gamma_{\ell J}) , \tag{43}$$

where

$$\gamma_{\ell J} = \frac{2}{\beta_{\ell J}^2} \equiv \frac{\Gamma_{\gamma,\ell} + \langle \Gamma_{n'} \rangle_{\ell J}}{\langle \Gamma_n \rangle_{\ell J}} . \tag{44}$$

In both cases the local average of the neutron width is given by

$$\langle \Gamma_n \rangle_{\ell J} = N_{\ell J} D_J S_\ell v_\ell (E) (E/E_1)^{1/2} \quad . \tag{45}$$

Since Eqs. 41 and 43 both show the same behavior for large and for small $\beta_{\ell J}$, i.e., for relatively large and small average neutron widths, we shall use the solution for $N_{\ell J} = 1$ for both cases (cf. Ref. 18). Then

$$\langle \sigma_\gamma \rangle = 2\pi^2 \lambda\!\!\!^{-2} \sum_{\ell=0}^{\infty} \frac{\Gamma_{\gamma,\ell}}{D_\ell} \frac{\sum_J g_J^2 [1 - \psi(0, \beta_{\ell J})}{\sum_J g_J^2} \quad . \tag{46}$$

If $\langle \Gamma_{n'} \rangle_{\ell J}$ does not depend on J (for example if it vanishes) one can use Eq. 35 to rewrite $\langle \sigma_\gamma \rangle$ as follows:

$$\langle \sigma_\gamma \rangle = 2\pi^2 \lambda\!\!\!^{-}\lambda\!\!\!^{-}_1 \sum_{\ell=0}^{\infty} (2\ell+1) S_\ell v_\ell \left\{ \frac{\Gamma_{\gamma,\ell}}{\Gamma_{\gamma,\ell} + \langle \Gamma_{n'} \rangle_\ell} \frac{\sum_J g_J^2 [1 - \psi(0, \beta_{\ell J})]}{\sum_J g_J^2 \beta_{\ell J}^2 / 2} \right\} \tag{47}$$

The same expression is approximately valid if $\langle \Gamma_{n'} \rangle_{\ell J} \approx 0$. At low energies, where $\langle \Gamma_n \rangle << \Gamma_\gamma$, the expression in square brackets approaches unity and $\langle \sigma_\gamma \rangle$ approaches $\langle \sigma \rangle - \sigma_p$. Equations 39 and 46 are used in the SESH code to calculate cross section averages analytically.

4.2 Average Transmission

The average transmission is not equal to the transmission which one would calculate from the average cross section:

$$\langle e^{-n\sigma} \rangle = e^{-n \langle \sigma \rangle} \langle e^{-n(\sigma - \langle \sigma \rangle)} \rangle$$

$$= e^{-n \langle \sigma \rangle} \left[1 + \frac{1}{2} n^2 \, \mathrm{var}[\sigma] - \frac{1}{6} n^3 (\sigma - \langle \sigma \rangle)^3 + - \ldots \right] \tag{48}$$

(n: sample thickness in nuclei/b; $\mathrm{var}[\sigma] = \langle \sigma^2 \rangle - \langle \sigma \rangle^2$: variance of the total cross-section distribution). The factor $e^{-n(\sigma - \langle \sigma \rangle)}$ is the analogue of the so-called self-shielding correction factor in the case of absorption (see Sect. 4.3). It is seen to arise from cross section fluctuations, approaching unity if the variance and the higher moments of the cross section distribution vanish and/or if the sample is very thin. As in Eq. 38 the average $\langle \ldots \rangle$ is defined as the energy average over an interval ΔE which contains a statistically meaningful sample of resonances but which is so narrow that the energy variation of the statistical parameters (average widths and level spacings) can be neglected.

One cannot hope to find analytical expressions for the average transmission because of its nonlinear dependence on the widths and spacings. On the other hand it is relatively easy to sample the width and spacing distributions in a Monte Carlo calculation. In this way one can generate samples of σ- and $e^{-n\sigma}$-values with the correct distributions and form the sample averages. This is the method adopted in the SESH code.

4.3 Average Probability for Detected Capture

The joint probability that: (1) a neutron with initial energy E is captured in a sample of thickness n, and (2) that the capture event is detected, can be written as

$$p(E,n) = \sum_{k=0}^{\infty} p_k(E,n) \, , \tag{49}$$

where $p_k(E,n)$ is the probability that detected capture occurs after exactly k scattering collisions in the sample. The first-collision capture probability is given by

$$P_0 = (1 - e^{-n\sigma}) \frac{\sigma_\gamma \varepsilon}{\sigma} \quad . \tag{50}$$

The multiple scattering terms p_1, p_2, ... are increasingly complicated functionals of σ and σ_γ (for more details see Section 5 and Ref. 19). The effective cross section for detected capture, $\sigma_\gamma \varepsilon$, is defined as in Eq. 20 above. It is even more hopeless than in the transmission case to find a closed expression for the average value of $p(E,n)$. Therefore, the Monte Carlo method is used to compute $\langle p(E,n) \rangle$ as an average. The multiple scattering terms p_1, p_2, etc. involve averages over scattering angles and free path distributions, cf. Sect. 5.2. These averages are also obtained by Monte Carlo techniques, as explained in Sections 5.2 and 6.6.

4.4 Average Self-indication Probability

Self-indication experiments are performed with two disc samples of the same material in the neutron beam. The first sample (thickness n_1) attenuates the beam, capture events in the second sample (thickness n_2) are detected. The probability that a neutron with energy E is captured in the second sample and that the capture event is detected can be written as

$$q(E,n_1,n_2) = e^{-n_1\sigma(E)} p(E,n_2) = e^{-n_1\sigma(E)} \sum_{k=0}^{\infty} p_k(E,n_2) \quad , \tag{51}$$

and in the unresolved-resonance region one measures the average $\langle q \rangle$. The code SESH can calculate this quantity also, in exact analogy to the Monte Carlo calculation of $\langle p \rangle$.

The Monte Carlo calculations are described in the next section.

5. MONTE CARLO CALCULATIONS

The basis of the Monte Carlo method is the fact that one can evaluate an integral of the form

$$y = \int_a^b dx\, w(x)\, f(x) \tag{52}$$

as an average. One considers w(x) as a weight distribution (which can also be uniform or a Dirac δ-distribution) and starts by generating values of x distributed according to w(x). Then one calculates for each x the corresponding value of f(x). Finally, one averages all f(x)-values obtained. The larger the sample of f(x)-values is, the closer the sample average will be (in the mean) to the exact value of the integral (52). The generalization to multi-dimensional integrals is straightforward.

The integrals which concern us here are the energy averages $\langle p \rangle$ and $\langle q \rangle$ of Section 4. They are calculated by the SESH code as averages over neutron "histories". Each history starts with a group of neutrons having unit weight and an energy E somewhere in the averaging interval ΔE. A history consists of a number of collisions. At each step the collision and escape probabilities are determined by the momentary cross sections and by geometry variables like the point of last interaction, the direction of the neutron path, and the distance to the sample surface in that direction. The cross sections are obtained by sampling the width and spacing distributions as described in Section 5.1. The geometry variables are found by sampling the angular distribution $(d\sigma_n/d\Omega)$ and the free path distribution as discussed in Section 5.2.

To calculate the average transmission $\langle e^{-n\sigma} \rangle$ all one has to do is to generate a sample of the cross-section distribution for the initial average energy $\overline{E}$ of ΔE.

5.1 Cross Section Sampling

Samples of the cross-section distributions are generated as follows: For a given energy $\overline{E}$, the average energy of the averaging interval ΔE, initial energies $E \approx \overline{E}$ are chosen for each neutron group. The energy E places the neutron group in a "resonance environment" as illustrated in Fig. 2. The resonance environment is generated from the level statistics at $\overline{E}$ as follows:

(1) The probability that E lies between two resonances of the J^{Π}-sequence such that the spacing has a value between D and D+dD is given by

$$p(D)\, dD \propto D p_J(D)\, dD \,, \tag{53}$$

where $p_J(D)\, dD$ is the Wigner distribution for the J-sequence (with mean spacing D_J). The extra factor D in Eq. 52 accounts for the fact that the number of neutrons falling in a given energy interval is proportional to the interval size D. In the SESH code D is obtained by sampling the distribution 53, then the difference between E and the lower bound of D is chosen at random between zero and D (because the neutron energy can lie anywhere in D with uniform probability).

(2) Next the reduced neutron widths for the two resonances defining the central interval D are found by sampling the Porter-Thomas distribution for all possible values of ℓ. The neutron width is then calculated according to Eq. 27 for even parity or the equivalent equation for odd parity.

(3) The contribution of these two resonances to σ, σ_n, and σ_γ can now be calculated from the Breit-Wigner formulae for isolated Doppler-broadened resonances (Eqs. 1, 2, 3, and 6).

(4) If the cross sections at $\overline{E}$ contain on the average appreciable contributions from more than two resonances additional resonances can be included in pairs - one resonance to the left, one to the right of the central interval for each pair (see Fig. 2).

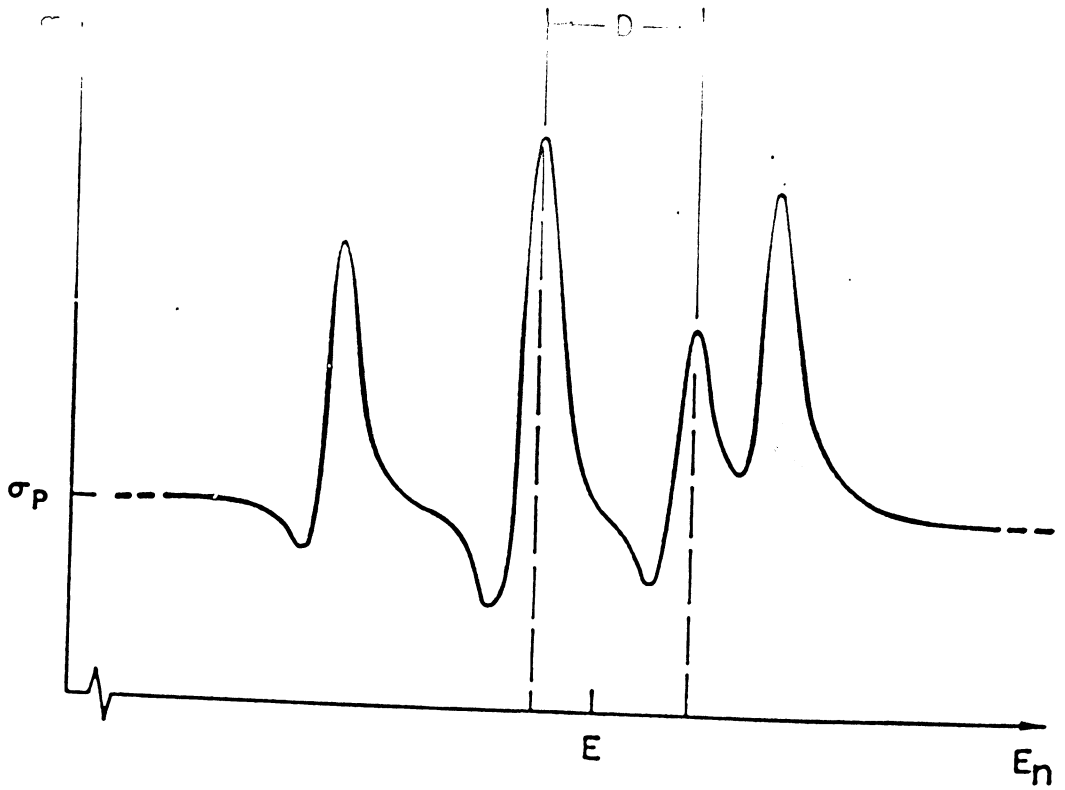

Fig. 2. Schematic illustration of "resonance environment" with central interval D and two resonance pairs.

This is accomplished by sampling the (pure !) Wigner distribution to get the level spacings, and the Porter-Thomas distribution to get the neutron widths. The number of resonance pairs is an input datum; two or three pairs are adequate in most cases.

(5) The above is done for all possible J^{Π}-sequences and all isotopes, and all the contributions are added according to Eqs. 19 and 20.

Having thus found σ_t, σ_n, σ_γ, and $\overline{\sigma_\gamma \epsilon}$ one can calculate collision probabilities and transmission, if the geometry variables are available. In the next sections it will be shown how the geometry variables are found.

5.2 Multiple-Scattering Calculation

In treating capture and self-indication data one must calculated the multiple-scattering terms p_1, p_2, ... of the collision expansion (49). At the energies of interest here we can account for the Doppler effect by simply using Doppler-broadened cross sections and by treating the target nuclei as stationary. For more detail see Ref. 20. We have to consider

(1) the probability that a neutron traverses a layer of material with "thickness" n without any interaction,

$$e^{-n\sigma} \equiv e^{-s} \tag{54}$$

(s is the thickness measured in mean free paths);

(2) the possibility that a neutron with a given energy is scattered elastically or inelastically in a thin layer of material,

$$(\sigma_n + \sigma_{n'})dn = \frac{\sigma_n + \sigma_{n'}}{\sigma} ds \equiv P_n ds \; ; \tag{55}$$

(3) the probability that an elastically scattered neutron travels within a solid angle element $d\Omega_c$ (CMS) after the collision

$$\frac{d\sigma_n(\theta_c, \varphi_c)}{\sigma_n} = \frac{1}{\sigma_n} \frac{d\sigma_n}{d\Omega_c} d\Omega_c \; . \tag{56}$$

(for inelastically scattered neutrons σ_n is to be replaced by $\sigma_{n'}$).

We shall approximate the actual angular distribution as isotropic, since s-wave scattering usually predominates in the energy range of interest here. Then

$$\frac{d\sigma_n}{\sigma_n} = \frac{d\Omega_c}{4\pi} = \frac{d(\cos\theta_c)}{2}\,\frac{d\varphi_c}{2\pi} \quad . \tag{57}$$

(4) Finally, we must consider the probability that the neutron is captured in a layer dn and that the capture event is detected,

$$dn\,\overline{\sigma_\gamma \epsilon} = \frac{\sigma_\gamma \epsilon}{\sigma} = P_\gamma ds \quad . \tag{58}$$

Using these probabilities and definitions one can write down the joint probabilities for capture after 0, 1, 2, ... scattering collisions. Summing over all possible neutron paths one finds

$$P_0 = P_{\gamma 0} \int_0^{S_0} ds_0 e^{-s_0} \quad , \tag{59.0}$$

$$P_1 = P_{n)} \int_0^{S_0} ds_0 e^{-s_0} \int_{4\pi} \frac{d\Omega_{c1}}{4\pi} P_{\gamma 1} \int_0^{S_1} ds_1 e^{-s_1} \quad , \tag{59.1}$$

$$P_2 = P_{n0} \int_0^{S_0} ds_0 e^{-s_0} \int_{4\pi} \frac{d\Omega_{c1}}{4\pi} P_{n1} \int_0^{S_1} ds_1 e^{-s_1} \int_{4\pi} \frac{d\Omega_{c2}}{4} P_{\gamma 2} \int_0^{S_2} ds_2 e^{-s_2} \quad , \tag{59.2}$$

etc.

The subscripts 0, 1, 2, ... refer to the number of scattering collisions which the neutron had already. The upper limits S_k (k=0, 1, 2, ...) are the maximal s_k-values, i.e., the distance in mean free paths between the point where the neutron had its k-th collision and the point where it would escape from the sample if there were no further interaction. The

S_k depends on the neutron velocity $\vec{v}_k$, which in turn depends on $\vec{v}_{k-1}$ and $\mu_{ck} = \cos\theta_{ck}$, which in turn depend on $\vec{v}_{k-2}$ and $\mu_{c,k-1}$, and so on. Of course the velocity, and hence the cross sections, change in every collision. Because of this complicated structure of the p_k only the simplest one, p_0, is readily calculated. Using $S_0 = n\sigma$ one finds just Eq. 50 above.

The dimensionality of the higher-order integrals increases as $3k + 1$ with the number k of scattering collisions. The only practical way to evaluate them is the Monte Carlo method. Comparison with Eq. 52 shows that this means sampling, for each collision, the distributions

$$w(s)\,ds = \frac{e^{-s}}{1 - e^{-S}}\,ds \quad , \quad 0 \le s \le S \; ; \tag{60}$$

$$w(\mu_c)\,d\mu_c = \frac{1}{2}\,d\mu_c \quad , \quad -1 \le \mu_c \equiv \cos\theta_c \le 1 \; ; \tag{61}$$

$$w(\varphi_c)\,d\varphi_c = \frac{1}{2\pi}\,d\varphi_c \quad , \quad 0 \le \varphi_c \le 2\pi \; . \tag{62}$$

These are the distributions for the number of mean free paths, s, between collisions, for the CMS colatitude θ_c and for the CMS azimuth φ_c of the post-collision direction with respect to the pre-collision direction of the scattered neutron. The scattering angles (and the post-collision excitation of the nucleus in inelastic collisions) determine the energy loss of the neutron. The cross sections and values of P_n and P_γ corresponding to each new energy are found as described in the previous section. Simulating a sufficient number of neutron histories and averaging the resulting capture probabilities from the 1st, 2nd, 3rd, ... interaction one finds $\langle p_0 \rangle$, $\langle p_1 \rangle$, $\langle p_2 \rangle$, ...

The kinematical equations needed for the calculation of θ, φ, E, and S from θ_c and φ_c are given in the following sections.

5.3 Elastic Scattering of Two Particles

We shall adopt the following conventions:

(1) Vectors will be denoted by an arrow ($\vec{v}$, Ω_c, ...), the corresponding magnitudes will be written without arrow (v, Ω_c, ...).

(2) Center-of-mass (CMS) quantities will be labeled by the subscript c (E_c, $\vec{v}_c$, μ_c, ...), the corresponding quantities in the laboratory system (LS) will be written without this subscript (E, $\vec{v}$, μ, ...).

(3) A prime will denote post-collision quantities (E', $\vec{v}'$, μ_c', ...), the corresponding pre-collision quantities will have no prime (E, $\vec{v}$, μ_c, ...).

Figure 3 shows the relation between the velocities $\vec{v}$ and $\vec{v}_c$ of the incoming neutron, $\vec{v}'$ and $\vec{v}_c'$ of the scattered neutron, and the velocity of the center of mass in the lab system, $\vec{v}_0$. Momentum conversation requires all these vectors to be coplanar, so that

$$\varphi = \varphi_c \ . \tag{63}$$

One has

$$\vec{v}_0 = \frac{\vec{v}}{A+1} \tag{64}$$

and

$$\vec{v}_c = \vec{v} - \vec{v}_0 \ , \tag{65}$$

$$\vec{v}_c' = \vec{v}' - \vec{v}_0 \ . \tag{66}$$

From these equations one derives easily

$$\mu = \frac{A\mu_c + 1}{(A^2 + 2A\mu_c + 1)^{1/2}} \ , \tag{67}$$

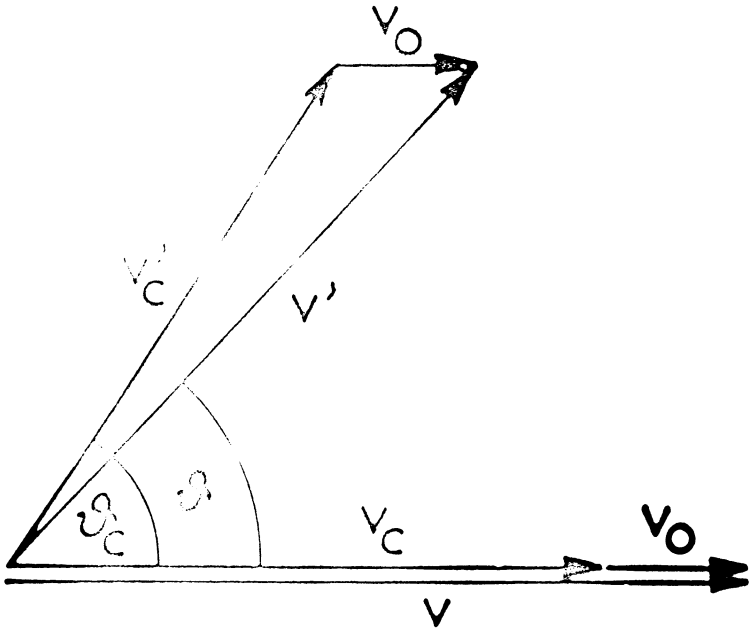

Fig. 3. LS and CMS velocities and scattering angles for stationary target nuclei.

$$E' = E \frac{A^2 + 2A\mu_c + 1}{(A+1)^2} \quad . \tag{68}$$

Equations 63 and 67 are used to calculate the LS scattering angles from the CMS scattering angles. The energy losses of elastically scattered neutrons with pre-collision energies E are uniformly distributed over the energy interval $E - \delta E \ldots E$, where

$$\delta E = E - E\left(\frac{A-1}{A+1}\right)^2 = E \frac{4A}{(A+1)^2} \quad . \tag{69}$$

In the SESH code, however, all post-collision energies are set equal to $E - \frac{1}{2}\delta E$, which means that the true energy loss is always replaced by the average energy loss. This quantity is usually much larger than the mean level spacing in the unresolved-resonance region. Therefore, we can take the post-collision resonance environment as completely uncorrelated to the pre-collision resonance environment.

The post-collision energy of inelastically scattered neutrons is also set equal to $E - \frac{1}{2}\delta E$ in the SESH code, which means that the excitation of the residual nucleus is neglected. There is no justification for this other than simplicity and convenience, and the code must be used with caution if inelastic scattering and multiple scattering are both relatively important. This is expected to be the case when the conditions (1) $\Gamma_{n'} \ll \langle \Gamma \rangle$, (2) ($\langle \Gamma_n \rangle \lesssim \Gamma_\gamma$ and $n\langle\sigma\rangle \lesssim 1$), are both unfulfilled.

From here on we shall discuss slab and spherical-shell geometry separately.

5.4 Slab Sample Geometry

Let us use as the LS a reference frame with its z-axis parallel to the beam direction. This reference frame will be fixed with respect to the sample. Let us further assume that we know the pre-collision direction $\vec{\Omega}$ of the neutron, the point where the last collision occurred, and the

scattering angles θ and φ. (See Fig. 4.) What is then the distance S to the sample surface? Before we can answer this question we must calculate the coordinates of the new direction, $\vec{\Omega}'$, from $\vec{\Omega}$, θ, and φ. We shall introduce an intermediate reference frame S'' which has its z''-axis parallel to $\vec{\Omega}$, so that in S''

$$\vec{\Omega} = \frac{\vec{v}}{v} = (0, 0, 1) , \tag{70}$$

$$\vec{\Omega}' = \frac{\vec{v}'}{v'} = (\sin\theta\cos\varphi, \sin\theta\sin\varphi, \cos\theta). \tag{71}$$

In the lab system we introduce polar angles by writing

in LS

$$\vec{\Omega} = (\Omega_x, \Omega_y, \Omega_z) = (\sin\zeta, \cos\eta, \sin\zeta\sin\eta, \cos\zeta). \tag{72}$$

In order to find the transformation which relates the S'' coordinates to the LS coordinates let us consider the following two rotations (Fig. 5):

(1) Rotation about the y''-axis, through an angle ζ,

$$\begin{pmatrix} x' \\ y' \\ z' \end{pmatrix} = \begin{pmatrix} \cos\zeta & 0 & \sin\zeta \\ 0 & 1 & 0 \\ -\sin\zeta & 0 & \cos\zeta \end{pmatrix} \begin{pmatrix} x'' \\ y'' \\ z'' \end{pmatrix} \tag{73}$$

(2) Rotation about the z''-axis, through an angle η

$$\begin{pmatrix} x \\ y \\ z \end{pmatrix} = \begin{pmatrix} \cos\eta & -\sin\eta & 0 \\ \sin\eta & \cos\eta & 0 \\ 0 & 0 & 1 \end{pmatrix} \begin{pmatrix} x' \\ y' \\ z' \end{pmatrix} . \tag{74}$$

Expressing the polar coordinates of $\vec{\Omega}$ by its Cartesian coordinates,

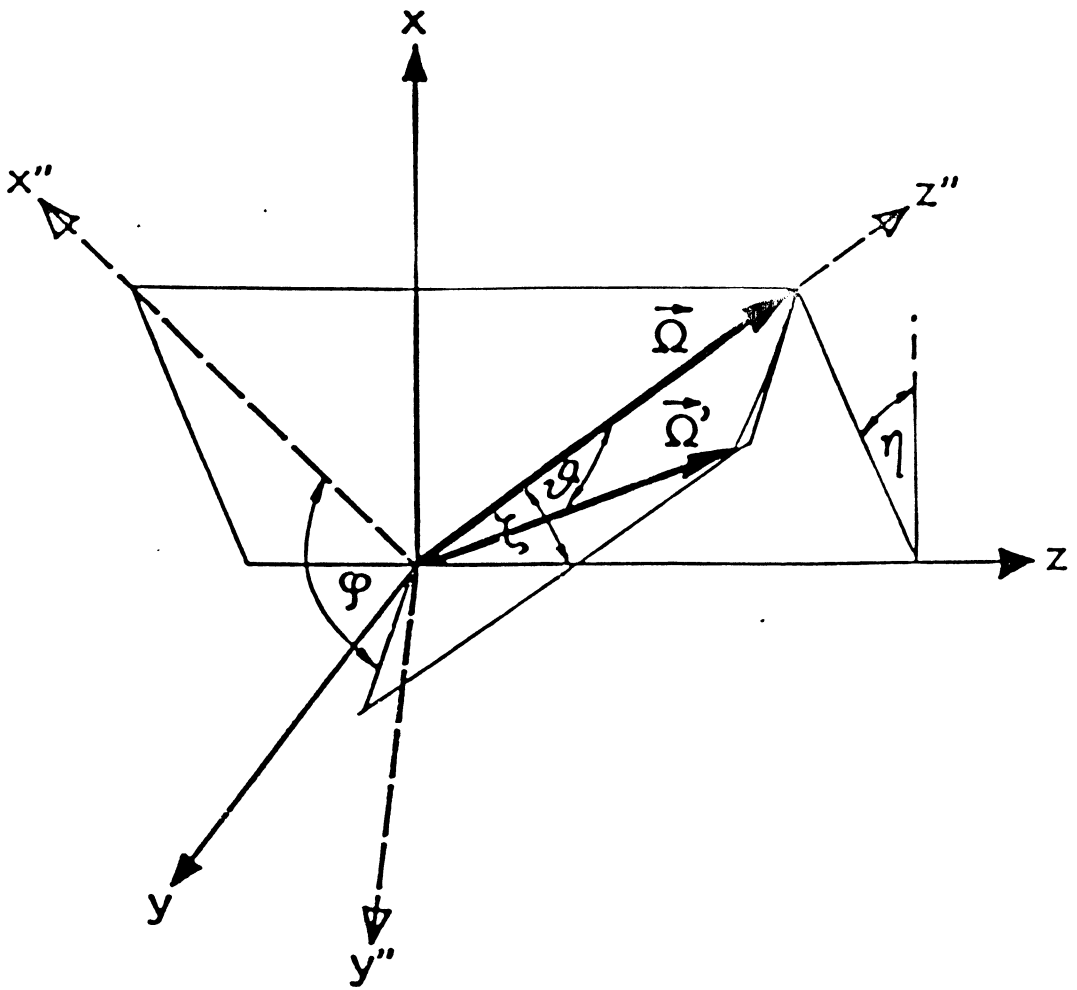

Fig. 4. Neutron directions $\vec{\Omega}$, $\vec{\Omega}'$ (before and after collision, resp.) and angles ζ, η, ϑ, φ, and their positions relative to the laboratory system (x, y, z) and to the system S'' (x'', y'', z''), in which $\vec{\Omega}$ has the coordinates (0, 0, 1).

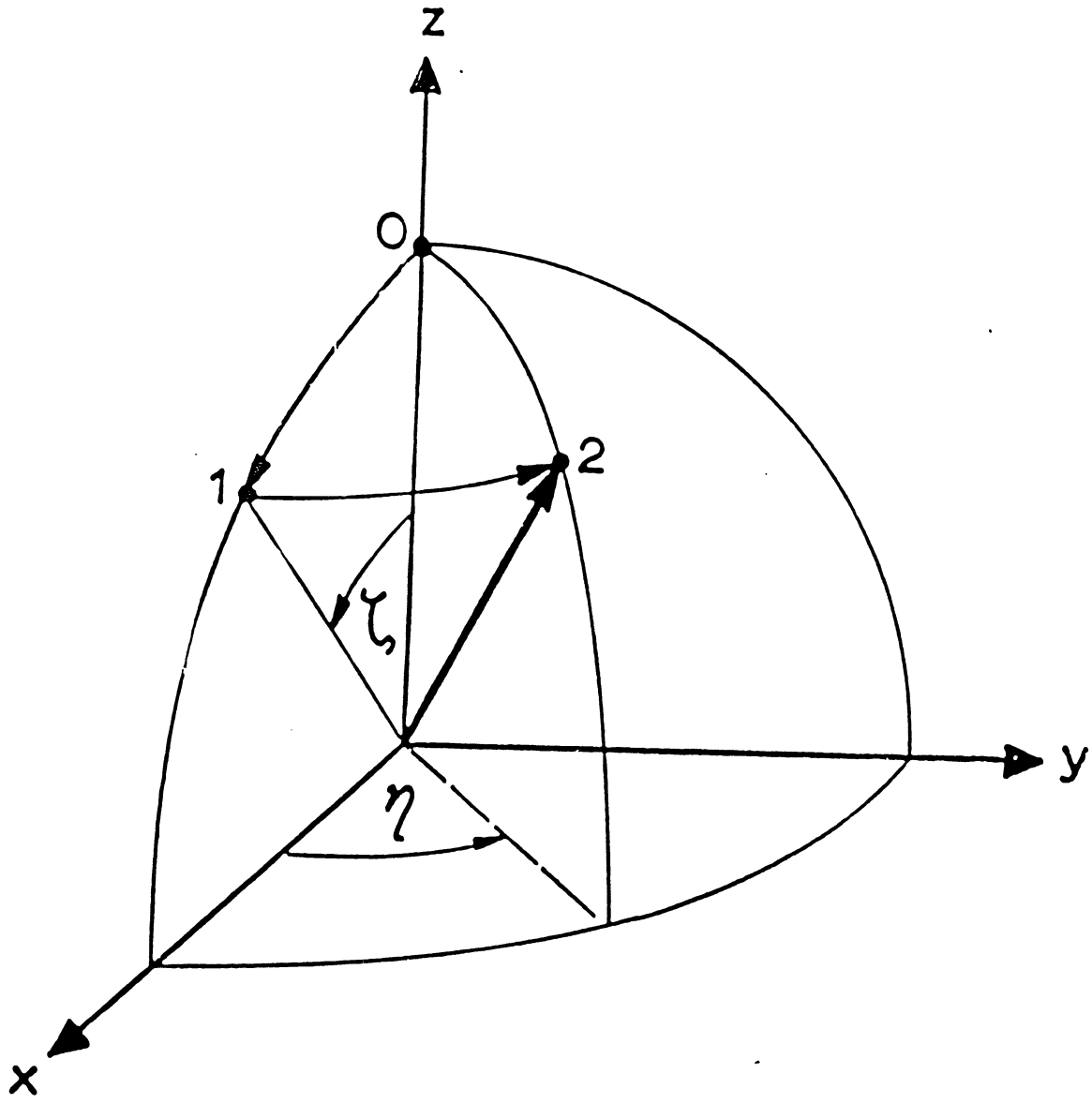

Fig. 5. Two-step rotation of a vector from the position (0, 0, 1) into the position ($\sin\zeta\cos\eta$, $\sin\zeta\sin\eta$, $\cos\zeta$).

$$\cos\zeta = \Omega_x , \qquad \cos\eta = \frac{\Omega_x}{\sqrt{1-\Omega_z^2}} ,$$

$$\sin\zeta = \sqrt{1-\Omega_z^2} , \quad \sin\eta = \frac{\Omega_y}{\sqrt{1-\Omega_z^2}} , \tag{75}$$

and combining the two transformations 73 and 74 one finds eventually for the LS coordinates of $\vec{\Omega}'$:

$$\begin{pmatrix} \Omega'_x \\ \Omega'_y \\ \Omega'_z \end{pmatrix} = \begin{pmatrix} \Omega_x\Omega_y(1-\Omega_z^2)^{-1/2} & -\Omega_y(1-\Omega_z^2)^{-1/2} & \Omega_x \\ \Omega_y\Omega_z(1-\Omega_z^2)^{-1/2} & \Omega_x(1-\Omega_z^2)^{-1/2} & \Omega_y \\ -(1-\Omega_z^2)^{1/2} & 0 & \Omega_z \end{pmatrix} \begin{pmatrix} \sin\theta\cos\varphi \\ \sin\theta\sin\varphi \\ \cos\theta \end{pmatrix} \tag{76}$$

In the special case $\Omega_z^2 = 1$ one cannot use this expression. In that case, however, the transformation is simply

$$\begin{pmatrix} \Omega'_x \\ \Omega'_y \\ \Omega'_z \end{pmatrix} = \Omega_z \begin{pmatrix} \sin\theta\cos\varphi \\ \sin\theta\sin\varphi \\ \cos\theta \end{pmatrix} \tag{77}$$

Equations 76 and 77 are used in the SESH code to calculate the direction of the neutron after the scattering collision.

We can now calculate the number of mean free paths, S, from the point of the last interaction to the sample surface, in the direction $\vec{\Omega}$. Let x_0, y_0, z_0 be the coordinates of the collision point. Then the equations of the neutron trajectory are

$$\frac{x-x_0}{\Omega_x} = \frac{y-y_0}{\Omega_y} = \frac{z-z_0}{\Omega_z} . \tag{78), (79}$$

The sample is taken as a cylindrical disc, with the cylinder axis parallel to the incident beam. Let the plain surfaces of the disc be described by

$$z = 0 \qquad \text{(front face)}, \tag{80}$$

$$z = Z \qquad \text{(back face)}, \tag{81}$$

and the cylindrical surface by

$$x^2 + y^2 = r^2 \tag{82}$$

The point where the neutron trajectory intersects the cylinder is defined by the solution (x, y, z) of Eqs. 78, 79, and 82, which can be written as

$$\begin{aligned} x &= x_0 + \Omega_x d_0 \\ y &= y_0 + \Omega_y d_0 \\ z &= z_0 + \Omega_x d_0 \ , \end{aligned} \tag{83}$$

with

$$d_0 = \frac{\sqrt{b^2 + ac} - b}{a} \ , \tag{84}$$

where

$$a \equiv \Omega_x^2 + \Omega_y^2 \ , \tag{85}$$

$$b \equiv x_0\Omega_x + y_0\Omega_y \ , \tag{86}$$

$$c \equiv r^2 - x_0^2 - y_0^2 \ .$$

The quantity d_0 is just the distance to the cylinder surface which we need. We must compare it to the distance to the front face,

$$d_1 = -\frac{z_0}{\Omega_z} \ , \tag{88}$$

if $\Omega_z < 0$, and to the distance to the back face,

$$d_2 = \frac{Z - z_0}{\Omega_z} , \tag{89}$$

if $\Omega_z > 0$. The smaller quantity in each case is the actual thickness of material, d, which the neutron has to traverse before it can escape from the sample:

$$d = \begin{cases} \min (d_0, d_1) & \text{if } \Omega_z < 0, \\ d_0 & \text{if } \Omega_z = 0 \\ \min (d_0, d_2) & \text{if } \Omega_z > 0 . \end{cases} \tag{90}$$

Finally S_k is given by

$$S_k = n\sigma(E_k) \frac{d}{Z} . \tag{91}$$

Of course

$$S_0 = n\sigma(E_0) . \tag{92}$$

5.5 Spherical-Shell Geometry

Let r_1 and r_2 denote the inner and the outer radius of a spherical-shell sample (Fig. 6). Let us further assume that the last (k-th) collision occurred at a distance r_0 from the center of the spherical sample, and let θ be the angle between the post-collision trajectory of the neutron and the radius r_0 (Fig. 6). Then it is easy to see that the maximal thickness of material in the way of the neutron is given by

$$d = r_0 \cos\theta + \sqrt{r_2^2 - r_0^2 \sin^2\theta} - 2u , \tag{93}$$

where

$$u = \begin{cases} \sqrt{r_1^2 - r_0^2 \sin^2\theta} & \text{if } \theta < \arcsin \frac{r_1}{r_0} , \\ 0 & \text{if } \theta \geq \arcsin \frac{r_1}{r_0} . \end{cases} \tag{94}$$

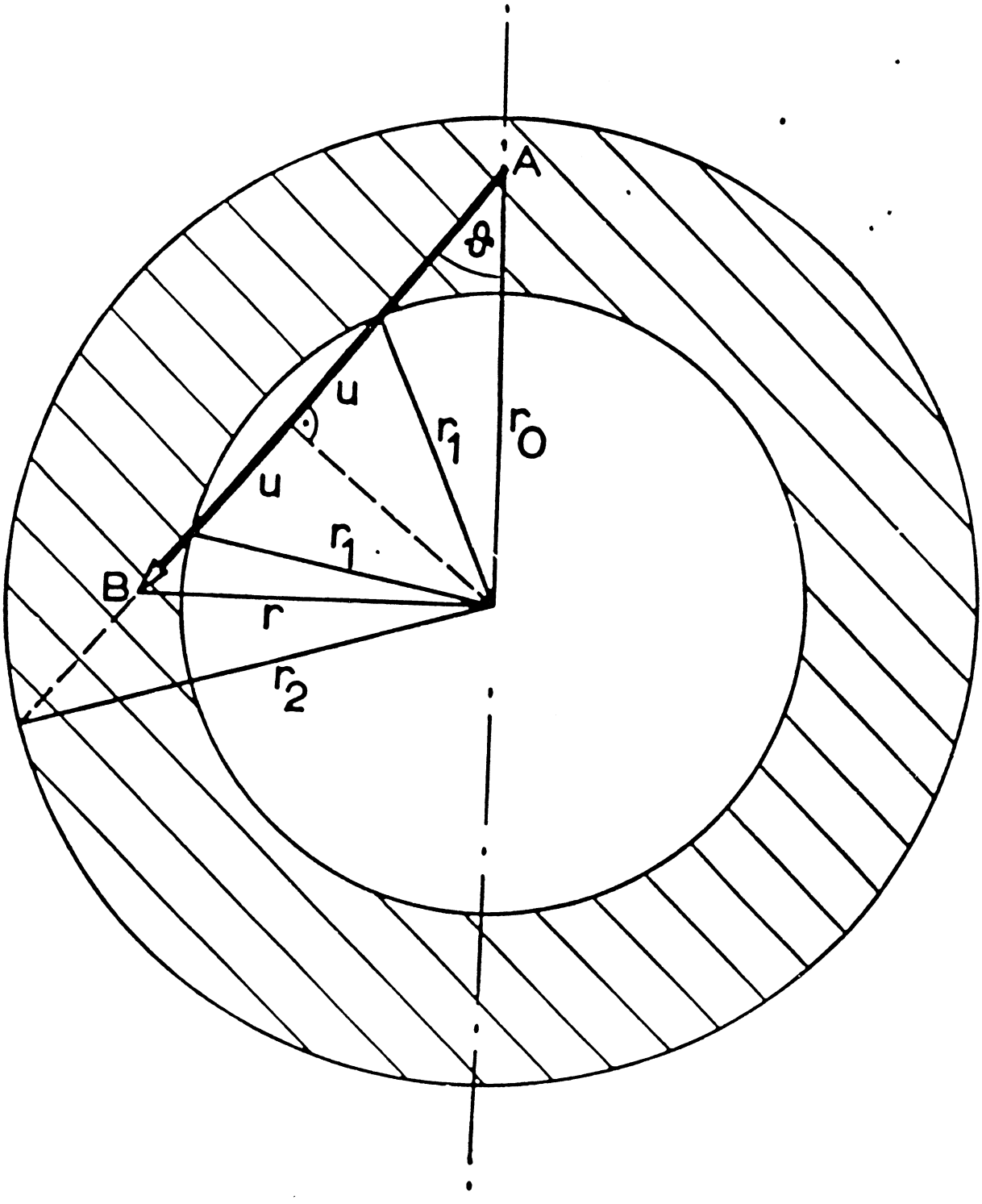

Fig. 6. Path of a neutron between collisions at points A and B (arrow) in spherical-shell geometry. The inner and outer shell radii are r_1 and r_2, the radius coordinates of A and B are r_0 and r. The angle ϑ and the quantities u used in the text are shown.

Expressing this distance in mean free paths one gets

$$S_k = n\sigma(E_k)\,\frac{d}{r_2 - r_1} \qquad \text{for } k > 0 \tag{95}$$

and

$$S_0 = n\sigma(E_0) \ , \tag{96}$$

where n is the thickness of the spherical shell in nuclei/b. Sampling the free path distribution (60) one finds s_k, and from s_k one can calculate the radial coordinate r of the point where the next collision occurs. The result is

$$r = \left[(s_k + 2u)^2 - 2(s_k + 2u)r_0 \cos\theta + r_0^2\right]^{1/2} . \tag{97}$$

In SESH the transformation from the CMS into the LS is avoided by neglecting the difference between the CMS and the LS angular distributions, and taking the LS angular distribution as isotropic. Since s-wave scattering usually predominates this approximation is quite adequate especially if the target nuclei are heavy ($A \gg 1$). One can then equate θ_c and θ, which means that one samples the distribution (61) directly for θ. The energy loss of a scattered neutron of initial energy E is again approximated by the average energy loss, $4AE(A+1)^{-2}$, as for disc sample geometry.

5.6 Error Estimation

The statistical uncertainties of the Monte Carlo averages are estimated as follows: Neutron histories are grouped (with 50 histories in each group), and the group averages x_i for a given quantity x are calculated as

$$x_i = \frac{1}{n_i} \sum_{j=1}^{n_i} x_{ij} \qquad (n_i = 50) \ , \tag{98}$$

where x_{ij} is the result of the j-th Monte Carlo history in the i-th group. The overall average is, of course,

$$\langle x \rangle = \frac{\sum_{i=1}^{N} n_i x_i}{\sum_{i=1}^{N} n_i} \quad , \tag{99}$$

N denoting the number of groups. The uncertainty of $\langle x \rangle$ is given by the square root of the variance, which is the expectation value of the quadratic deviation,

$$\mathrm{var}[x] = \langle (x - \langle x \rangle)^2 \rangle \approx \frac{1}{N(N-1)} \sum_{i=1}^{N} (x_i - \langle x \rangle)^2 \quad . \tag{100}$$

The transmission or the probability for detected capture are examples for the quantity x. The self-shielding correction factors are ratios of averages, of the form

$$y(x_\mu, x_\nu) = \frac{x_\mu}{x_\nu} \qquad (\mu \neq \nu) \tag{101}$$

(we use Greek letters to distinguish different statistical variables, Roman letters to distinguish neutron histories and history groups). The variance of a function of two statistical variables must be calculated as

$$\mathrm{var}[y(x_1, x_2)] \approx \sum_{\mu=1}^{2} \sum_{\nu=1}^{2} \frac{\partial y}{\partial x_\mu} C_{\mu\nu} \frac{\partial y}{\partial x_\nu} \quad , \tag{102}$$

where

$$C_{\mu\nu} = C_{\nu\mu} = \langle (x_\mu - \langle x_\mu \rangle)(x_\nu - \langle x_\nu \rangle) \rangle$$

$$= \begin{cases} \mathrm{var}[x_\mu] & \text{if } \mu = \nu \ , \\ \mathrm{cov}[x_\mu, x_\nu] & \text{if } \mu \neq \nu \ . \end{cases} \qquad (103)$$

The $C_{\mu\nu}$ are the elements of the error (or covariance) matrix. The covariances are calculated as

$$\mathrm{cov}[x_1, x_2] \approx \frac{1}{N(N-1)} \sum_{i=1}^{N} (x_{1i} - \langle x_1 \rangle)(x_{2i} - \langle x_2 \rangle) \qquad . (104)$$

in SESH.

6. THE CODE

Having reviewed the necessary formulae we can now describe the code itself. A FORTRAN list is presented as Appendix A to this document. The main purpose of the code is to calculate any one of the following quantities:

average transmission	$\langle e^{-n\sigma(E)} \rangle$,
average probability for detected capture	$\langle p(E,n) \rangle$,
average self-indication probability	$\langle e^{-n_1\sigma(E)} p(E,n_2) \rangle$,

where $\langle \ldots \rangle$ denotes local energy averages or, equivalently, averages over the local level spacing and width distributions. In addition, SESH calculates the following cross section averages, both analytically and by Monte Carlo methods:

average total cross section	$\langle \sigma(E) \rangle$,
average effective capture cross section	$\langle \overline{\sigma_\gamma(E)\epsilon(E)} \rangle$.

The end result consists of the correction factors

$$C_T = \frac{\langle e^{-n\sigma(E)} \rangle}{e^{-n \langle \sigma(E) \rangle}} , \tag{105}$$

$$C_C = \frac{\langle p(E,n) \rangle}{n \langle \sigma_\gamma(E)\epsilon(E) \rangle} , \tag{106}$$

$$C_S = \frac{\langle e^{-n_1\sigma(E)} p(E,n_2) \rangle}{e^{-n_1 \langle \sigma(E) \rangle} n_2 \langle \overline{\sigma_\gamma(E)\epsilon(E)} \rangle} . \tag{107}$$

These are the correction factors that are needed in the analysis of transmission, capture, and self-indication data, resp., in the unresolved-energy region. The SESH code is tailored to the requirements in the energy range of roughly 5 keV to 500 keV for medium-weight and heavy nuclei. The correction factors are calculated from known or estimated statistical parameters. This means that the code is not a search code in the sense that it yields statistical resonance parameters from experimental data by some sort of fitting procedure. Of course, one can vary the SESH input until a measured set of data is fitted by the results, and as a matter of fact a least-squares program, SFIT,[21] was written which uses SESH correction factors to fit transmission data by adjusting s- and p-wave strength functions.

The cross sections calculated from the statistical parameters appear in the output as: (1) analytical results, and (2) as Monte Carlo averages. Both must agree within the statistical uncertainties of the Monte Carlo calculation. Lack of agreement is usually due to an insufficient number of resonance pairs in the Monte Carlo construction of resonance environments.

The code can handle problems with up to 10 nuclides, up to four partial waves (s, p, d, f) per nuclide, and up to five sample geometries in any combination.

6.1 Input

The input is read from punched cards. Table 2 shows the formats used.

1. The first card is a title card which may contain arbitrary alphanumeric information identifying the problem, such as date, run number, nuclide(s), sample thickness(es), etc. A tag on the title card can be used to specify whether cross section and other statistical distributions are to be printed in tabular form.

2. The cards following the title card consist of groups, one group for each nuclide. The first card of each group contains information on the nuclide (A, a, U_0, Θ, T, I; see Table 2). The other cards of each group are partial-wave cards containing the ℓ-dependent quantities $\Gamma_{\gamma,\ell}$, D_ℓ, S_ℓ, S'_ℓ (strength function for inelastic scattering), R, and c_ℓ, as explained in Table 2. There is one card for each partial wave, interpreted by the computer as belonging to $\ell = 0, 1, 2, 3$, in the order in which the cards are read. One can omit the one, two, or three highest-order partial waves in the calculation by simply leaving out the last one, two, or three partial-wave cards. Up to 10 nuclides can be handled.

3. Following the nuclide and partial-wave cards there are three cards specifying the geometries (disc or spherical shell) and thicknesses for up to five samples. The first one of these three cards contains sample thicknesses, the second one outer radii (i.e., cylinder radii for disc samples), and the third one inner radii for spherical-shell samples or transmission sample thicknesses for self-indication calculations. All thicknesses and radii must be given in nuclei/b. The input on the three "sample cards" is used by the computer to identify the type of problem according to the following scheme:

Table 1

n	r_2	r_1	Type of Problem
> 0	0	0	Average Transmission
> 0	> 0	0	Average Capture, Disc Sample
> 0	> 0	> 0	Self-indication, Disc Samples
0	> 0	> 0	Average Capture, Spherical Shell

As stated above, r_1 is interpreted as the thickness of the transmission (filter) sample for self-indication calculations.

4. The next card contains the number of resonance pairs which are to be used in the construction of resonance environments (see Sect. 5.1.).

TABLE 2. INPUT SCHEME

Column	Format	Symbol	Units	Explanatory Remarks
1. Title Card				
1-72	12A6	--	--	arbitrary alphanumeric input
73-80	18	τ	--	tag for calculation and pointout of distributions of $\sigma, \overline{\sigma_\gamma \epsilon}$, p, $e^{-n\sigma}$ $\tau = 0$: no distributions needed $\tau = 1$: distributions needed
2. Nuclide Groups				1 group per isotope, ≤ 10 isotopes
2.1 Nuclide Card				
1-10	E10.5	A Target	--	ratio of nuclear mass to neutron mass
11-20	"	a	--	isotopic abundance
21-30	"	U_o	MeV	effective neutron-binding energy (Ref. 14)
31-40	"	Θ	MeV	effective nuclear temperature (Ref. 14)
41-50	"	T	^oK	effective sample temperature (Ref. 8)
51-60	"	I	--	spin of target ground state
2.2 Partial-Wave Card				1 card for each ℓ-value, in the order $\ell = 0, 1, \ldots, \ell_{max}; 0 \leq \ell_{max} \leq 3$
1-10	E10.5	$\Gamma_{\gamma,\ell}$	eV	average radiation width near neutron threshold
11-20	"	D_ℓ	eV	average level spacing near neutron threshold
21-30	"	S_ℓ	--	strength function for elastic scattering


```
C
C  GILBERT-CAMERON COMPOSITE LEVEL DENSITY AND GIANT DIPOLE RESONANCE
C  MODEL ARE USED FOR THE ENERGY DEPENDENCE OF LEVEL SPACINGS AND
C  RADIATION WIDTHS IN VERSION 1975. THE INPUT REMAINS AS DESCRIBED
C  IN GA-8380 WITH TWO EXCEPTIONS: (1) THE NUCLEAR TEMPERATURE IS
C  REPLACED BY THE GILBERT-CAMERON PAIRING ENERGY OF THE COMPOUND
C  NUCLEUS, (2) ONLY THE S-WAVE LEVEL SPACING MUST BE GIVEN (SPACING
C  INPUT FOR L>0 IS IGNORED). FURTHERMORE, CHANNEL RADIUS AND
C  EFFECTIVE NUCLEAR RADIUS ARE DISTINCT FOR ALL PARTIAL WAVES:
C  THE CHANNEL RADIUS IS TAKEN AS RC(I)=(1.23*A**(1/3)+0.80) FM,
C  THE EFFECTIVE NUCLEAR RADII R(L,I) ARE INPUT NUMBERS WITH THE
C  DEFAULT VALUES R(L,I)=RC(I).
```

TABLE 2. INPUT SCHEME (cont)

Column	Format	Symbol	Units	Explanatory Remarks
31-40	E10.5	S'_ℓ	--	strength function for inelastic scattering[a)]
41-50	"	R'	fm	effective nuclear radius
51-60	"	ϵ_ℓ	--	efficiency of capture detector
3. Geometry Cards				specifying up to 5 different sample geometries
3.1 Card for Sample Thicknesses				
11-60	5E10.5	n	nuclei/b	see Table 1
3.2 Card for Outer Radii				
11-60	5E10.5	r_2	nuclei/b	see Table 1
3.3 Card for Inner Radii				
11-60	%E10.5	r_1	nuclei/b	see Table 1
4. Card for Number of Resonance Pairs				
1-10	E10.5	N_P	--	number of pairs for "resonance environments"
5. Energy Cards				≤ 34 cards with ≤ 100 energies
1-10	E10.5	$\overline{E}$	keV	average energy
11-20	"	N_H	--	number of Monte Carlo histories
21-30	"	$\overline{E}$	keV	average energy
31-40	"	N_H	--	number of Monte Carlo histories
41-50	"	$\overline{E}$	keV	average energy
51-60	"	N_H	--	number of Monte Carlo histories

Brian McDermott added a 4th geometry card to specify neutron beam size on sample: columns 11-60, 5E10.5 format, in nuclei/b

TABLE 2. INPUT SCHEME (cont)

Column	Format	Symbol	Units	Explanatory Remarks
61-70	E10.5	$\overline{E}$	keV	average energy
71-80	"	N_H	--	number of Monte Carlo histories
6. Blank Card				signals end of problem .

Note: The first 10 columns of these geometry cards must be blank. The number of Monte Carlo histories should be multiples of 50. Problems can be stacked.

5. The next cards contain up to 100 pairs of energies $\overline{E}$ and numbers of Monte Carlo histories to be used in the Monte Carlo calculations.

6. The end of the problem is signalled to the computer by a blank card.

Problems can be stacked by simply putting the cards of the next problem behind the cards of a preceding problem. Each problem of the stack must begin with a title card and end with a blank card.

6.2 The Main Program

After the input is read from the punched cards the contents of the title card and of all nuclide and partial-wave cards are printed, arranged in essentially the same way as on the cards.

Then, average total and capture cross sections (Eqs. 4, 39, and 46) for all isotopes and energies are calculated and printed. Next the Monte Carlo calculation of the energy averages is done for all sample geometries and input energies. For this purpose one of the Monte Carlo subroutines MOCT, MUSC, or MUSS is called, MOCT for transmission calculations, MUSC for capture and self-indication calculations with cylindrical samples, MUSS for capture calculations in spherical geometry. The Monte Carlo results are then printed, as discussed in more detail below.

6.3 Subroutine ENDEP

Subroutine ENDEP yields factors which describe the energy dependence of the mean level spacings and average radiation widths. For the level spacing we use the simple Boltzmann factor of Eq. 33 as proposed by Gilbert and Cameron for excitation energies below about 10 MeV.[14]

The energy dependence of the average radiation width is assumed to be described by

$$\Gamma_\gamma(E) = \Gamma_\gamma(0)\, e^{-E/\Theta} \frac{P\left(\frac{U}{\Theta}\right)}{P\left(\frac{U_0}{\Theta}\right)} , \qquad (108)$$

with

$$U = U_0 + E \tag{109}$$

and

$$P(x) \equiv 6 + 6x + 3x^2 + x^3 \ , \tag{110}$$

where U_0 is the effective binding energy, and Θ the nuclear temperature. Tables of both quantities can be found in Ref. 14. Typical values are $U_0 \sim 7$ MeV, $\Theta \sim 0.5$ MeV. It is usually sufficient to use rough numbers for U_0 and Θ since the calculations are not very sensitive to these quantities. Equations 108 - 110 follow from the dipole approximation

$$\Gamma_\gamma(E) \propto D(U) \int_0^U \frac{E_\gamma^3 dE_\gamma}{D(U-E_\gamma)} \tag{111}$$

(see Refs. 22, 23) and Eq. 33 by straightforward integration.

6.4 Subroutine PEPS

PEPS provides hard-sphere penetrability factors (Eq. 15) and phase shifts (Eq. 7) for the cross section calculations.

6.5 Subroutine MOCT

The Monte Carlo subroutine MOCT calculates average transmissions $\langle e^{-n\sigma} \rangle$ by generating cross sections as described in Sect. 5.1. and averaging the corresponding transmission. The statistical uncertainties of the average transmission and of the transmission correction factor C_T (Eq. 105) are calculated as discussed in Sect. 5.6. Monte Carlo averages of the cross sections are also calculated.

6.6 Subroutine MUSC

MUSC calculates the quantities $\langle p(E,n) \rangle$ or $\langle e^{-n_1\sigma(E)} p(E,n_2) \rangle$ and C_C (Eq. 106) or C_S (Eq. 107), resp. As in MOCT cross section averages are also calculated. The cross section sampling is performed

as described in Sect. 5.1, and the Monte Carlo calculation of multiple scattering is done as described in Sections 5.2., 5.3., 5.4. Neutron histories are simulated by sampling the free path distribution (60) and the angular distributions (61), (62). After finding the resonance environment for the incident neutron one can calculate p_0 (Eq. 50). The product

$$\left(1 - e^{-n\sigma}\right)\left(1 - \frac{\sigma_\gamma}{\sigma}\right) = \left(1 - e^{-S_0}\right)P_{n0} \qquad (112)$$

(compare Eq. 59) represents the chance that the neutron survives the first collision unescaped (first factor) and unabsorbed (second factor). The neutron history is now terminated if the neutron does not "survive" Russian roulette played with the survival probability (112). Russian roulette is simulated by comparing a random number from the interval 0...1 with $(1-e^{-S_0})P_{n0}$. If the neutron survives, the location of the last collision is found by sampling (60) for s_0, and the scattering angles by sampling (61) and (62). The LS angles and the new direction are calculated with Eqs. 63, 67, and 76. Next the distance to the sample surface is found (Eqs. 84 - 90). The new cross sections are then computed under the assumption that the energy loss is large compared to the mean level spacing, so that no correlation exists between the new and the old cross sections. The contribution of the singly scattered flux is, on the average,

$$\langle p_1 \rangle = \left\langle \left(1 - e^{-S_0}\right)P_{n0} \left(1 - e^{-S_1}\right)P_{\gamma 1} \right\rangle . \qquad (113)$$

Note that the first two factors are actually realized by Russian roulette. From here on everything is repeated: Russian roulette with survival chance $(1-e^{-S_1})P_{n1}$, picking of location and angles for the second collision, sampling of cross sections and calculation of distance to sample surface, etc., etc. The history is terminated as soon as the neutron does not

survive Russian roulette. If this happens after the k-th collision, this particular history yields a contribution

$$p = p_0 + p_1 + \ldots + p_{k-1} \tag{114}$$

with (on the average)

$$\langle p_o \rangle = \left\langle \left(1 - e^{-S_0}\right) P_{\gamma 0} \right\rangle , \tag{115.0}$$

$$\langle p_1 \rangle = \left\langle \left(1 - e^{-S_0}\right) P_{n0} \left(1 - e^{-S_1}\right) P_{\gamma 1} \right\rangle \tag{115.1}$$

$$\langle p_2 \rangle = \left\langle \left(1 - e^{-S_0}\right) P_{n0} \left(1 - e^{-S_1}\right) P_{n1} \left(1 - e^{-S_2}\right) P_{\gamma 2} \right\rangle \tag{115.2}$$

etc.

where all factors $(1 - e^{-S_k}) P_{n0}$ are actually realized by Russian roulette. The average number of collisions over all histories and the statistical uncertainties (see Sect. 5.6.) are calculated for the printout, and then control is transferred back to the main program.

Self-indication probabilities are calculated in essentially the same way. One averages over $e^{-n\sigma} p$ instead over p, the exponential factor being the transmission of the first (filter) sample.

6.7 Subroutine MUSS

MUSS differs from MUSC only insofar as spherical-shell instead of disc geometry is used (see Sect. 5.5.), and that no self-indication calculation is done.

6.8 Subroutines AVER, AVERT, AVERP

These subroutines are used in grouping histories in groups of 50 histories for the error estimation.

6.9 Subroutines PFCN, PFCNP

PFCN and PFCNP are used in the calculation of the Doppler shape functions ψ and φ (Eqs. 8, 9). These functions occur in the cross section Eqs. 1 - 3 and in the expression for the average capture cross section (Eq. 46). It should be mentioned that most of the execution time for typical SESH calculations is spent in the evaluation of ψ and φ. Various schemes were tried, including interpolation between stored values, and the combination PFCN plus PFCNP is the outcome. Each one of these two subroutines is used in the domain where it is fastest. Actually PFCNP is the FORTRAN IV version of a SHARE subroutine[24] which was originally used in SESH. PFCN is a subroutine which uses the method described in Ref. 25, and which is somewhat faster and more accurate in various domains of the x,β-plane. Both PFCN and PFCNP yield values of the real and imaginary part of the complex probability integral $W = U + iV$, and ψ and φ are then calculated according to

$$\psi(x,\beta) + i\varphi(x,\beta) = \frac{\sqrt{\pi}}{\beta} W\left(\frac{x+i}{\beta}\right) = \frac{\sqrt{\pi}}{\beta}\left[U\left(\frac{x}{\beta},\frac{1}{\beta}\right) + iV\left(\frac{x}{\beta},\frac{1}{\beta}\right)\right] , \tag{116}$$

where

$$W(z) = \frac{1}{\pi i}\int_{-\infty}^{\infty} \frac{e^{-s^2}}{s-z}\, ds \quad . \tag{117}$$

6.10 Subroutines PORTER, WIGNER, and SPACE

These subroutines sample the Porter-Thomas, Wigner, and modified Wigner distributions (Eqs. 21, 28, and 53, respectively).

The cumulative Wigner distribution is

$$P(D) = \int_0^D p(D)\, dC = 1 - e^{-x^2}, \quad x = \frac{\sqrt{\pi}}{2}\frac{D}{D_J} \quad . \tag{118}$$

Solving for D one obtains

$$D = \frac{2}{\sqrt{\pi}} D_J [- \ln(1 - P(D))]^{1/2} \quad . \tag{119}$$

This shows that one can generate the distribution p(D) dD by sampling random numbers n from a uniform distribution between 0 and 1, and calculating D from Eq. 119, setting 1 - P(D) = n.

In the case of the Porter-Thomas and of the modified Wigner distribution one cannot invert the functional relationship between the cumulative probability distribution and its argument in such a simple manner. Therefore we use the rejection technique (v. Neumann, Ref. 26) to generate the distributions. Since the rejection scheme requires a bounded range of the variable, we transform from the range 0...∞ into the range 0...1 as follows:

$$0 \leq x = \frac{1}{2} \frac{\Gamma_n^l}{\langle \Gamma_n^l \rangle} \leq \infty \rightarrow 0 \leq \xi = \left(\frac{x}{1+x}\right)^{1/2} \leq 1$$

in PORTER, and

$$0 \leq x = \frac{\sqrt{\pi}}{2} \frac{D}{D_J} \leq \infty \rightarrow 0 \leq \eta = \frac{x^3}{1+x^3} \leq 1$$

in SPACE. With these transformations we avoid the usual truncation and the errors caused by it. The particular forms of the transformations were chosen in an attempt to maximize the efficiency of the rejection scheme.

6.11 Function RANDOM (X)

This is the generator of (pseudo-) random numbers between 0 and 1 which is used in all Monte Carlo sampling operations.

6.12 Printout

The printout consists of essentially three parts. An example is shown in Appendix B. First the contents of the title card, then that of the nuclide and partial-wave cards are printed. After the analytical cross section calculation the analytical results are written. The last part consists of the Monte Carlo results, including error estimates, and of the relevant input data (sample thicknesses, numbers of Monte Carlo histories and of resonance pairs).

7. SAMPLE PROBLEM

In Appendix B we show an example of a SESH calculation. Self-shielding corrections were calculated for capture data taken with 0.036 in. of rhenium, with 85% Re^{187}. The printout shows the contents of the title first and, then, under the heading INPUT, the contents of two groups of cards corresponding to the two isotopes Re^{185} and Re^{187}. Each group contains two partial-wave cards which means that s- and p-wave neutrons are considered only. The analytical results show that this is sufficient below about 5 keV, but above this energy the p-wave capture cross section becomes gradually more important than the s-wave capture cross section. Therefore, it would have been better to include d-wave capture also. The Monte Carlo results show, for the cross sections, good agreement (within the error bars) with the analytical results. The self-shielding correction factor C_c is smaller than one below ~ 2 keV mainly because of the opacity of the sample. Above 2 keV the first sum term in

$$C_c = \sum_{k=0}^{\infty} \frac{\langle P_k(E_1 n)\rangle}{n\langle \sigma_\gamma(E)\epsilon\rangle} \tag{120}$$

becomes practically equal to 1, because the sample becomes more and more transparent (see last column), and the multiple scattering contributions push C_c above unity. The accuracy of C_c at low energies is not very good with the chosen number of 1000 histories, above 2 keV; however, it is about 3%, which is close to the value $1000^{-1/2}$ expected for relatively smooth cross sections and small multiple scattering contributions. This calculation required 45 minutes on the UNIVAC 1108 computer.

REFERENCES

1. H. A. Bethe, J. R. Beyster and R. E. Carter, J. Nucl. Energy, 3, (1956) 207.

2. L. Dresner, Nucl. Instr. Methods, 16 (1962) 176.

3. R. L. Macklin, Nucl. Instr. Methods, 26 (1964) 213.

4. D. Bogart and T. T. Semler, Conference on Neutron Cross Section Technology, 1966, Washington, D. C., USAEC Report CONF-660303, Book 1, p. 502.

5. D. Bogart, Nuclear Data for Reactors, Paris, 1966, IAEA Report CONF-661014-41, Vol. I, p. 503.

6. H. Feshbach, C. E. Porter and V. F. Weisskopf, Phys. Rev. 96, (1954) 448.

7. H. A. Bethe and G. Placzek, Phys. Rev. 51 (1937) 450; see also: M. Born, "Optik," Berlin 1933; and: F. H. Fröhner, Nucl. Instr. Methods, 49 (1967) 89.

8. W. E. Lamb, Phys. Rev. 55 (1939) 190.

9. C. E. Porter and R. G. Thomas, Phys. Rev. 104 (1956) 483.

10. W. M. Lopez, E. Haddad, S. J. Friesenhahn and F. H. Fröhner, Nucl. Phys. A93 (1967) 340.

11. J. D. Garrison, Annals of Physics, 30 (1964) 269.

12. E. P. Wigner, Oak Ridge Report ORNL-2309 (1957) p. 59; see also: M. L. Mehta, Nucl. Phys. 18 (1960) 395.

13. H. Hurwitz and H. A. Bethe, Phys. Rev. 81 (1951) 898; see also: T. D. Newton, Can. J. Phys. 34 (1956) 804.

14. A. Gilbert and A. G. W. Cameron, Can. J. Phys. 43 (1965) 1446.

15. Julien, de Barros. Bianchi, Corge, Huynh, le Poittevin, Morgenstern, Netter, Samour, and Vastel, Nucl. Phys. 76 (1966) 391.

16. Julien, de Barros, Chevillon, Huynh, Morgenstern, Netter, and Samour, Nuclear Data for Reactors, Paris, 1966, IAEA Report CONF-661014-41, Vol. I, p. 205.

17. K. K. Seth, Nucl. Data, A2 (1966) 299.

18. J. D. Garrison and B. W. Roos, Nucl. Sci. Eng. 12 (1962) 115.

19. F. H. Fröhner and E. Haddad, Nucl. Phys. 71 (1965) 129.

20. F. H. Fröhner, "TACASI - A FORTRAN IV Code for Least Squares Area Analysis of Neutron Resonance Data," USAEC Report GA-6906, General Atomic Division, General Dynamics Corporation (1966).

21. J. M. Blatt and V. F. Weisskopf, Theoretical Nuclear Physics, New York (1952).

22. A. G. W. Cameron, Can. J. Phys. 35 (1957) 666.

23. W. Gautschi and A. Beam, SHARE Subroutine BS WOFZ, National Bureau of Standards Report, 1957.

24. M. R. Bhat and G. E. Lee-Whiting, Nucl. Instr. Meth. 47 (1967) 277.

25. J. V. Neumann, Nat. Bur. Stand., Appl. Math. Series 12 (1951) 36.